In vivo Imaging of the Systemic Recruitment of Fibroblasts to the Angiogenic Rim of Ovarian Carcinoma Tumors

Dorit Granot,[1] Yoseph Addadi,[1] Vyacheslav Kalchenko,[2] Alon Harmelin,[2] Leoni A. Kunz-Schughart,[3] and Michal Neeman[1]

Departments of [1]Biological Regulation and [2]Veterinary Resources, Weizmann Institute, Rehovot, Israel and [3]OncoRay—Center for Radiation Research in Oncology, Medical Faculty Carl Gustav Carus, Technical University of Dresden, Dresden, Germany

Abstract

Tumor-associated stroma, in general, and tumor fibroblasts and myofibroblasts, in particular, play a role in tumor progression. We previously reported that myofibroblast infiltration into implanted ovarian carcinoma spheroids marked the exit of tumors from dormancy and that these cells contributed to vascular stabilization in ovarian tumors by expression of angiopoietin-1 and angiopoietin-2. *Ex vivo* labeling of fibroblasts with either magnetic resonance or optical probes rendered them detectable for *in vivo* imaging. Thus, magnetic resonance imaging (MRI) follow-up was feasible by biotin-bovine serum albumin-gadolinium diethylenetriaminepentaacetic acid or iron oxide particles, whereas labeling with near-IR and fluorescent vital stains enabled *in vivo* visualization by near-IR imaging and two-photon microscopy. Using this approach, we show here that prelabeled fibroblasts given i.p. to CD-1 nude mice can be followed *in vivo* by MRI and optical imaging over several days, revealing their extensive recruitment into the stroma of remote s.c. MLS human epithelial ovarian carcinoma tumors. Two-photon microscopy revealed the alignment of these invading fibroblasts in the outer rim of the tumor, colocalizing with the angiogenic neovasculature. Such angiogenic vessels remained confined to the stroma tracks within the tumor and did not penetrate the tumor nodules. These results provide dynamic evidence for the role of tumor fibroblasts in maintenance of functional tumor vasculature and offer means for image-guided targeting of these abundant stroma cells to the tumor as a possible mechanism for cellular cancer therapy. [Cancer Res 2007;67(19):9180–9]

Introduction

Epithelial ovarian cancer is the most lethal of all gynecologic cancers. Although ovarian cancer is not as abundant as breast, colon, or prostate carcinoma, it accounts for the highest mortality rate with 5-year survival of only 44%. The poor prognosis is mostly dominated by the advanced stage at the time of diagnosis, at which metastases have already formed in inner organs such as the kidneys and intestines (1). Surface epithelium ovarian cancer is the prominent type of ovarian cancer and accounts for ~90% of all ovarian tumors (benign and malignant; ref. 2). This surface epithelium layer participates in the ovulation process, both actively through the secretion of proteolytic enzymes and cytokines as well as mechanically as the initial site of tissue degeneration. The incidence of ovarian epithelium cancer increases with numerous ovulation events that do not lead to pregnancy. Reactive oxidants produced at the ovulation wound during ovulation promote DNA aberrations in the surface epithelium cells, which consequently become more susceptible to transformation. Hence, the "incessant ovulation" hypothesis was introduced. The theory claims that pregnancy and lactation protect against ovarian cancer, whereas repeated ovulations without long cessation periods facilitate malignancy (2, 3).

Despite the link between ovulation and ovarian cancer, the prevalence and severity of the disease are highest in postmenopausal women. Thus, there seems to be a long latency period between transformation of the ovarian epithelial cells and progression of ovarian cancer. This etiology of ovarian cancer led to the "hormonal hypothesis," linking ovarian carcinoma with hormonal changes that accompany menopause and particularly implicating the gonadotropin hormones, luteinizing hormone and follicle-stimulating hormone, in tumor progression (4). We previously showed that implanted ovarian carcinoma tumors respond to gonadotropin stimulation indirectly by induction of adhesion and angiogenesis (5, 6). In the absence of these stimuli, implanted ovarian carcinoma spheroids show extended dormancy characterized by futile cycles of angiogenesis and vascular regression, which could be detected by magnetic resonance imaging (MRI; refs. 7, 8). Thus, tumor-derived vascular endothelial growth factor (VEGF) was sufficient for inducing angiogenesis but not sufficient for vascular maintenance in a manner that would support tumor growth. Exit from dormancy was marked by infiltration of stroma cells and particularly myofibroblasts, which promoted vascular stability and functionality by expression of angiopoietin-1 and angiopoietin-2 (9).

The role of fibroblasts in ovarian cancer progression is consistent with previous reports that fibroblasts have a fundamental role in pathologic circumstances such as wound healing and tumor progression (10, 11). Coinoculation of fibroblasts with tumor cells promoted tumor progression and angiogenesis in prostate cancer (12, 13), ovarian cancer (12, 14), and breast cancer (15). The tumor stroma, also referred to as "reactive stroma," is correlated with desmoplasia (i.e., increase in fibroblastic cell population, capillaries, inflammatory cells, collagen type I, and fibrin deposition; ref. 16). The desmoplastic reaction is characterized by pronounced alterations in the phenotype and expression profile of the associated fibroblastic cells (17), such as expression of α smooth muscle actin (α-SMA), which have thus have been termed as myofibroblasts (18).

Homeostasis of epithelium is achieved through balanced signaling cascades via factors that are secreted by both epithelial

Note: Supplementary data for this article are available at Cancer Research Online (http://cancerres.aacrjournals.org/).

Requests for reprints: Michal Neeman, Department of Biological Regulation, Weizmann Institute, Rehovot 76100, Israel. Phone: 972-8-934-2487; Fax: 972-8-9346264; E-mail: michal.neeman@weizmann.ac.il.

doi:10.1158/0008-5472.CAN-07-0684

and stromal cells and that exert their functions through paracrine and autocrine mechanisms (11, 19). Fibroblasts are the major constituents of the connective tissue and, to a high degree, are responsible for synthesis of extracellular matrix components and formation of basement membrane. Immunohistochemistry of invasive endometrial tumors showed myofibroblast staining for growth factors related to angiogenesis and tumorigenesis (20).

Angiogenesis is a basic requirement for solid tumor growth and progression because all solid tumors, regardless of their origin, require stroma for their progression. In contrast to the normal blood vessels, tumor vessels are characteristically immature, tortuous, and chaotically scattered, forming leaky, poorly functioning endothelial channels, either devoid or loosely attached to periendothelial cells and are more dependent on VEGF for their survival (21).

Recent studies suggested that matrix-bound fibroblasts enhance angiogenesis as well as endothelial cell motility (22). Interactions between endothelial cells and fibroblasts in three-dimensional cocultures of human umbilical vein endothelial cells (HUVEC) and human primary fibroblasts revealed temporal and spatial organization, in which the endothelial cells composed the inner mass of the spheroid whereas fibroblasts were typically located at the periphery (14, 22–24). Additionally, human skin fibroblasts were recently shown to support the migration and tube formation of HUVEC in a three-dimensional culture system (25).

Recruitment of fibroblasts to tumor stroma is governed by molecular factors that are only partly known. Platelet-derived growth factor (PDGF) secreted by tumor cells can be recognized by the PDGF receptor on the mesenchymal cells and has been shown to participate in the recruitment of pericytes to maturing blood vessels (15). It is likely that myofibroblasts are recruited from different sources as cancer formation progresses (11, 26, 27). During initial tumor stages, it was suggested that myofibroblasts differentiate from the local fibroblast population in the epithelial stroma on transforming growth factor (TGFβ1) stimulation, whereas at later tumor progression stages, myofibroblasts are recruited from distant locations (28–32). Green fluorescent protein–positive bone marrow–derived fibroblasts were recruited to both s.c. and i.p. tumors in mice (33). Furthermore, fibroblasts that originated from various organs such as skin, lung, and bone

Table 1. Experiment design

Experiment	Experimental design (no. mice)	Analysis	Figure(s)
(I) S.c. MLS tumors	(*a*) MLS cells (5×10^6); (*b*) coinoculation MLS + CV-1 (2×10^6); (*c*) MLS followed by CV-1 (s.c.); (*d*) MLS followed by CV-1 (i.p.); $n = 12$	H&E	1
(II) Retention of the label in primary fibroblasts	PFN2, normal breast–derived fibroblasts labeled/unlabeled with biotin-BSA-GdDTPA ($n = 9$)	MRI, 3D-GE	S1
(III) Local recruitment, MRI	Tumors were initiated before s.c. administration of fibroblast; CV-1 cells (2×10^6) labeled with biotin-BSA-GdDTPA ($n = 6$)	MRI, 3D-GE, H&E	2
(IV) Systemic recruitment (MRI)	Tumors were initiated before i.p. administration of fibroblast; (*a*) CV-1 cells (2×10^6) labeled with biotin-BSA-GdDTPA ($n = 10$); (*b*) CV-1 cells labeled with 0.75 mg/mL Feridex ($n = 4$)	MRI, 3D-GE, H&E Prussian blue staining.	3
(V) Systemic recruitment (near-IR)	Tumors labeled with DiASP initiated before i.p. administration of fibroblast; CV-1 cells (2×10^6) prelabeled with DiR ($n = 7$)	Near-IR imaging	4
(VI) Fibroblasts distribution in the tumor	DiD/CFSE-labeled tumors initiated before i.p. fibroblast administration; blood vessels were imaged by i.v. injection of dextran-FITC. CV-1 cells labeled with DiI, DiD, or CFSE ($n = 8$) Coinoculation of tumor cells and fibroblasts ($n = 2$)	Fluorescence imaging, two-photon microscopy	5, S2, S3
(VII) Systemic recruitment of human primary fibroblasts	Tumors were initiated from MLS cells or MLS transfected with yellow fluorescent protein before i.p. administration of normal breast-derived ($n = 3$) and lung-derived ($n = 2$) human fibroblasts (PFN2 and WI38, respectively) prelabeled with Feridex (PFN2) or DiI (WI38)	Fluorescence imaging, MRI and histology, Prussian blue and α-SMA stainings	6

Abbreviation: 3D-GE, three-dimensional gradient-echo.

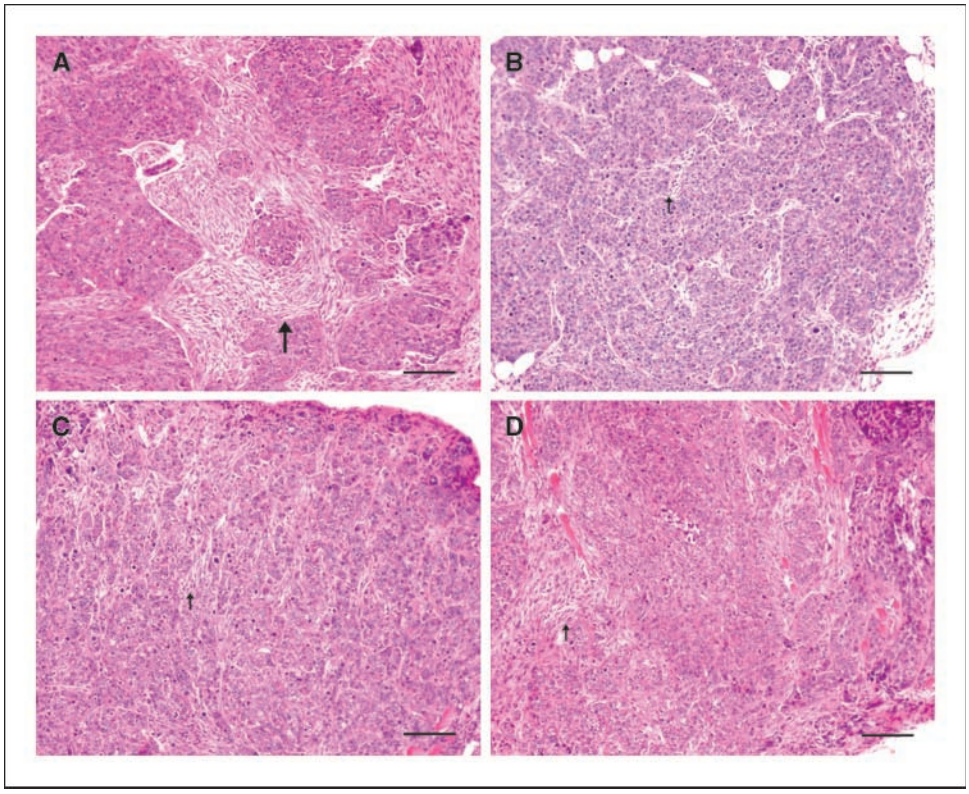

Figure 1. Desmoplasia in s.c. human epithelial ovarian carcinomas. H&E staining of MLS tumors generated in the hind limb of CD-1 nude mice (Table 1, *Exp I, a–d*). *A,* tumors formed by s.c. inoculation of MLS cells. *B,* MLS cells coinoculated along with CV-1 fibroblasts. *C,* CV-1 fibroblasts injected s.c. adjacent to s.c. MLS tumors. *D,* i.p. administration of CV-1 fibroblasts into tumor-bearing mice. *Arrows,* fibrosis.

marrow showed different efficiencies of fibroblasts recruitment into i.p. ovarian tumors (34). In this context, myofibroblastic modulation seems to depend on complex environmental network, in which TGFβ1 is significantly, but not exclusively, involved (35).

The aim of the study reported here was to track the systemic recruitment of fibroblasts into tumors by MRI/near-IR imaging. MRI has become a favorable tool for noninvasive tracking of cells (22, 36). The vast majority of cell labeling studies for MRI use superparamagnetic iron oxide particles. Labeled cells are typically detected through the large magnetic susceptibility effect, resulting in easily detectable signal void. Conversely, paramagnetic metal ions such as gadolinium (Gd^{3+}) mainly affect T_1 relaxation rate of the surrounding water, thus enhancing the MRI signal of the labeled cells in comparison with nearby tissue (37–39). Recently, MRI was applied for tracking of endothelial precursor cells (EPC) that are involved in tumor angiogenesis and vascular remodeling using iron oxide nanoparticles (40, 41) and Gd-HPDO3A caged in apoferritin (42). We reported recently the use of biotin-bovine serum albumin (BSA)-gadolinium-diethylenetriaminepentaacetic acid (GdDTPA) for *ex vivo* labeling of tumor fibroblasts (43). In the study reported here, *in vivo* MRI and near-IR imaging allowed detection of the recruitment of i.p. administered fibroblasts into s.c. ovarian carcinoma tumors. The recruited cells colocalized with the neovasculature at the tumor rim, suggesting the role of these stroma cells in tumor angiogenesis and their possible use for image-guided cellular targeting of tumors.

Materials and Methods

Cell culture. Primary PFN2 fibroblasts were obtained from a poorly differentiated invasive G3 breast tumor (44). Fibroblasts were cultured from frozen stocks in DMEM with a cumulative population doubling of <40. Assays were done using primary fibroblasts of passages 3 to 7. The human ovarian epithelial carcinoma cell line MLS and the normal monkey kidney fibroblast cell line CV-1 were cultured in α-MEM. WI38 human primary lung fibroblasts were cultured in Eagle's MEM. All media were supplemented with 10% FCS (Beit Haemek), 100 units/mL penicillin, 0.1 mg/mL streptomycin, 0.06 mg/mL amphotericin B, and 2 mmol/L L-glutamine.

Tumor models. Animal experiments were approved by the Weizmann Institutional Animal Care and Use Committee. S.c. MLS tumors were generated by inoculation of 3×10^6 to 5×10^6 MLS cells into the hind limb of the mouse under anesthesia [75 mg/kg ketamine i.p. (Fort Dodge Animal Health); 3 mg/kg xylazin i.p. (XYL-M2, V.M.D.)]. Several experimental designs were used (Table 1). At the end of the imaging experiments, animals were sacrificed and tumor samples were removed and fixed in either Carnoy's solution (6:3:1 ethanol/chloroform/acetic acid) or 10% formaldehyde for H&E and Prussian blue stainings, respectively. Specimens were additionally stained for α-SMA expression.

Cell labeling. Fibroblasts were labeled *in vitro* with either biotin-BSA-GdDTPA (10 mg/mL; generating T_1 contrast) or Feridex (0.75 mg/mL, Advanced Magnetics; generating T_2* contrast). Biotin-BSA-GdDTPA was synthesized and r_1 relaxivity was determined as previously described (45) and was found to be 186 $(mmol/L)^{-1}\ s^{-1}$ [6.8 $(mmol/L)^{-1}\ s^{-1}$ per GdDTPA]. Labeling was done by the addition of contrast material (either Feridex or biotin-BSA-GdDTPA) into the culture media for 48-h incubation and was followed by extensive washes in PBS.

Fluorescent and near-IR vital stains. CV-1 fibroblasts were labeled with 3.5 μg/mL of 1,1′-dioctadecyl-3,3,3′-tetramethylindotricarbocyanine iodide (DiR; Molecular Probes, Inc.) by addition of the dye into cells suspended in PBS (46). After 30-min incubation at 37°C, cells were extensively washed in PBS. For double fluorescence imaging of tumors and fibroblasts, MLS cells were stained as well with 7.5 μg/mL of 4-(4-(didecylamino)styryl)-*N*-methylpyridium iodide [4-Di-10-ASP; Molecular Probes].

Cells (tumor or fibroblasts) were labeled with carboxymethyl-1,1′-dioctadecyl-3,3,3′,3′-tetramethylindocarbocyanine (CM-DiI; 7.5 μg/mL; CellTracker, Molecular Probes); 1,1′-dioctadecyl-3,3,3′,3′-tetramethylindodicarbocyanine, 4-chlorobenzenesulfonate salt (DiD; 7.5 μg/mL); or

carboxyfluorescein diacetate, succinimidyl ester (CFSE; 5 μmol/L; Molecular Probes). Cell pellets were suspended in final concentrations in PBS and labeling was achieved by 1-h incubation, followed by extensive washes in PBS.

MRI studies. MRI was done on a horizontal 4.7-T Biospec spectrometer (Bruker) using a whole-body birdcage transmission coil. *In vivo* MRI measurements for detection of biotin-BSA-GdDTPA–labeled fibroblasts were done on CD-1 mice with s.c. tumors. A series of T1-weighted three-dimensional gradient-echo images, with pulse flip angles of 5, 15, 30, 50, and 70 degrees, were acquired to determine R_1 values [repetition time (TR), 10 ms; echo time (TE), 3.56 ms (two averages); spectral width, 50,000 Hz; field of view, 6 × 6 × 3 cm, 128 × 128 × 64 pixels; total acquisition time per frame, 163 s]. Three-dimensional gradient-echo data sets were used for generation of R_1 maps as well as for calculation of the average R_1 values in selected regions of interest (Supplementary Fig. S1) by nonlinear best fit to the equation

$$I = \frac{M_0 \sin\alpha(1 - e^{-\mathrm{TR}*R_1})}{1 - \cos\alpha e^{-\mathrm{TR}*R_1}}$$

where I is the signal intensity as a function of the pulse flip angle. Student's t test (two-tailed, equal variance) was used for statistical analysis of the significance of change in relaxation rate between control and labeled tumors.

Feridex-labeled fibroblasts were detected in T_2* weighted three-dimensional gradient-echo images (TE, 10 ms; TR, 13.56 ms; flip angle, 15 degrees, four averages; spectral width, 50,000 Hz; field of view, 6 × 6 × 3 cm, 128 × 128 × 64 pixels; zero filled to 256 × 256 × 256).

Near-IR and fluorescence imaging. *In vivo* near-IR images were acquired using IVIS 100 (Xenogen). The excitation and emission filter sets for DiR fluorescence were 710 to 760 and 810 to 860 nm, respectively. The excitation and emission filter sets for DiASP were 445 to 490 and 515 to 575 nm, respectively. Mice were visualized 1 to 10 days after administration of fibroblasts. At the end point of the experiment, tissues were excised and imaged as well.

Two-photon microscopy of tumors. S.c. MLS tumors were initiated in CD-1 nude mice by inoculation of 5 × 10^6 DiD- or CFSE-prelabeled MLS cells. After 4 days, 2 × 10^6 DiI- or CFSE-prelabeled CV-1 fibroblasts were injected into the peritonea of tumor-bearing mice. Imaging of the vasculature was obtained by i.v. injection of 0.2-mL dextran-FITC (2 mg/mouse; 500 KD; Sigma) before sacrifice of the mice. Excised tumors were placed in glycerol and imaged immediately by two-photon microscopy (2PM; Zeiss LSM 510 META NLO; equipped with a broadband Mai Tai-HP-femtosecond single box tunable Ti-sapphire oscillator, with automated broadband wavelength tuning 700–1,020 nm from Spectraphysics, for two-photon excitation).

Results

Desmoplasia in s.c. MLS human ovarian carcinoma tumors. Ovarian carcinomas are characteristically fibrotic; hence, we assessed whether this phenomenon is conserved in s.c. xenograft tumors. Tumors were generated in the hind limb of CD-1 nude mice from MLS human ovarian carcinoma cells (Table 1, *Exp I, a*). H&E stainings of tumor specimens showed the high abundance of fibrotic tissue within the tumor mass (Fig. 1*A*). Similar appearance was observed for tumors initiated from MLS cells coinoculated along with fibroblasts, or when the fibroblasts were administered either s.c. or i.p. subsequent to tumor establishment (Fig. 1*B–D*; Table 1, *Exp I, b–d*). Thus, in s.c. MLS tumors, the microenvironment undergoes desmoplastic reaction that is manifested by the large fibroblast cell population in the tumor milieu. Exogenous administration of fibroblasts did not alter the tumor pathology.

Prolonged *in vivo* visibility of *in vitro* labeled fibroblasts. We have previously reported the short term (1–2 days) *in vivo* MRI

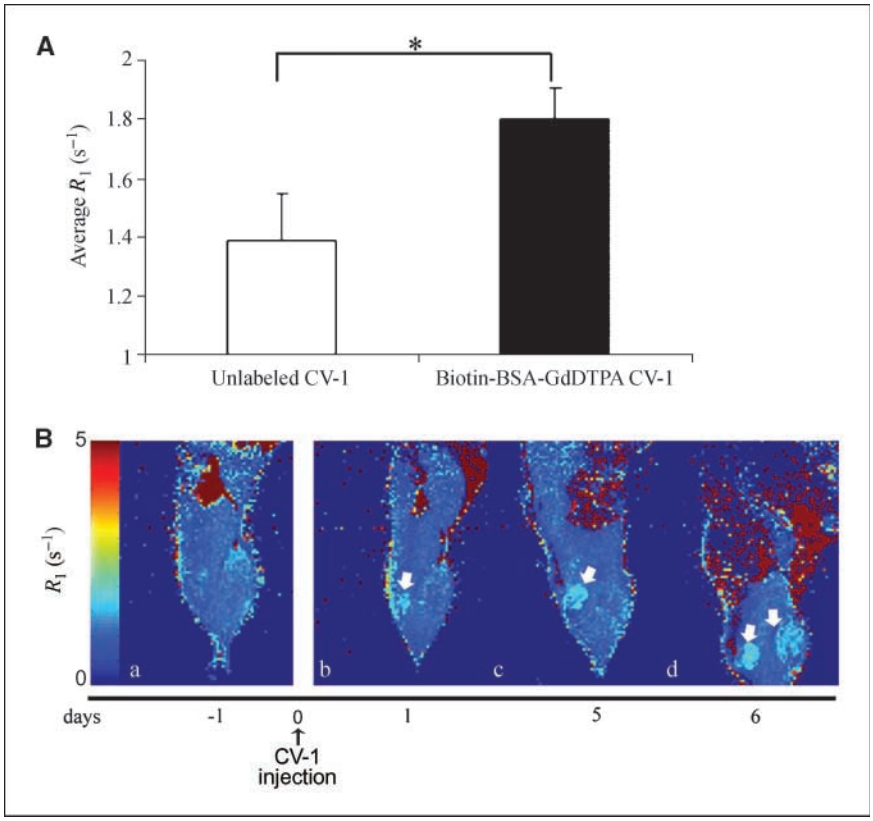

Figure 2. Local recruitment of fibroblasts into s.c. tumors. Tumors were initiated in the hind limb of CD-1 nude mice by s.c. inoculation of MLS cells (3 × 10^6) followed by an adjacent s.c. injection of biotin-BSA-GdDTPA–labeled or unlabeled CV-1 fibroblasts (2 × 10^6; Table 1, *Exp III*). *A, columns,* average R_1 values obtained from region of interest analysis of the tumor regions 6 d after s.c. injection of labeled (*black column*) or unlabeled (*white column*) cells (n = 3 for each group); *bars,* SE. *, P < 0.05, significant change in R_1 of labeled versus unlabeled tumors (one-tailed, unpaired t test). *B,* R_1 maps of one representative tumor scanned over several days. *a,* R_1 map of the tumor before injection of labeled CV-1. R_1 maps 1 d (*b*), 5 d (*c*), and 6 d (*d*) after injection of labeled fibroblasts. Note the migration of labeled fibroblasts from the right tumor lobe to the left (*arrows*).

visibility of fibroblasts prelabeled *in vitro* with biotin-BSA-GdDTPA (43). Here, we evaluated the feasibility for prolonged MRI tracking of biotin-BSA-GdDTPA–labeled fibroblasts (Table 1, *Exp II*). Tumors were generated in nude mice by coinoculation of MLS cells along with PFN2 primary fibroblasts that were either prelabeled (10 mg/mL biotin-BSA-GdDTPA, 48 h) or unlabeled. The visibility of prelabeled fibroblasts was determined by MRI measurements of R_1 of the tumors. MRI data were acquired 1 and 8 days after inoculation of labeled and control tumors (n = 5 and n = 4, respectively). R_1 values were significantly elevated in tumors with labeled fibroblasts both 1 and 8 days after inoculation (Supplementary Fig. S1). Thus, not only was a small fraction of labeled cells (10%) in the tumor volume visible after inoculation but the contrast significantly persisted for at least 8 days *in vivo*.

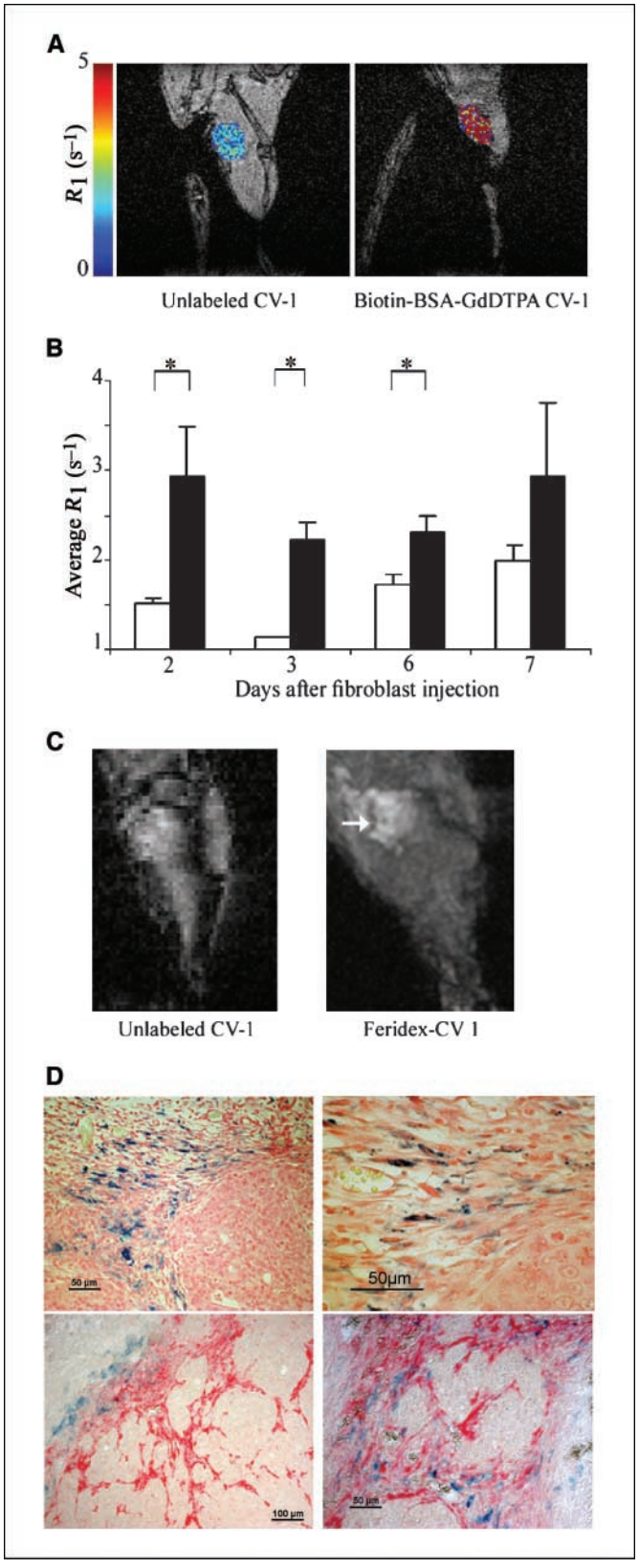

***In vivo* MRI detection of local fibroblast recruitment into tumors.** Local recruitment of labeled cells into the tumor region was monitored by R_1 measurements of tumors before and after injection of prelabeled fibroblasts (Table 1, *Exp III*). Fibroblasts (CV-1; labeled or unlabeled) were administered into s.c. tissue at an adjacent site to the tumor ($\sim$2 mm from the tumor rim). R_1 values were significantly elevated for tumors in which the administered fibroblasts were prelabeled with biotin-BSA-GdDTPA (Fig. 2). Six days after s.c. injection of labeled fibroblasts, the average R_1 value of tumors was $\sim 1.8 \pm 0.1\ s^{-1}$ (n = 3) whereas it was only $1.4 \pm 0.1\ s^{-1}$ (n = 3) in tumors with unlabeled fibroblasts (Fig. 2*A*; $P < 0.05$). Moreover, follow-up MRI studies revealed increased R_1 5 and 6 days after injection of labeled cells and showed evidence for migration of the labeled fibroblasts within the tumor (Fig. 2*B, b–d, arrows*).

***In vivo* MRI detection of systemic fibroblast recruitment into tumors.** Systemic recruitment of fibroblasts to the tumor was studied by MRI using CV-1 fibroblasts prelabeled with biotin-BSA-GdDTPA (Table 1, *Exp IV*). Fibroblasts (2×10^6 CV-1 cells, labeled or unlabeled; n = 5 for each group) were administered into the peritonea of mice with established s.c. MLS tumors in the hind limb. R_1 values of tumors following i.p. injection of prelabeled fibroblasts were greater than the ones observed in the presence of unlabeled fibroblasts (Fig. 3*A*; $P < 0.05$). Recruitment of fibroblasts was detectable as early as 2 days after administration of cells, and the elevated R_1 values persisted for 6 days. However, 7 days after injection of labeled cells, the increase in R_1 was no longer significant. During the 6 days of measurement, tumor size increased from $\sim$3 to 6.5 mm in diameter. Calculation of the change in R_1 ($\Delta R_1 = R_{1(\text{labeled})} - R_{1\ (\text{control})}$) suggested a similar (no significant difference) ΔR_1 for local ($0.42\ s^{-1}$; Fig. 2) and systemic ($0.66\ s^{-1}$; Fig. 3) recruitment of fibroblasts (P = 0.39).

To further validate that the signal arising at the tumor site can be attributed to the recruited fibroblasts and to exclude the possibility that the label was transferred from dying fibroblasts to phagocytic cells, we labeled CV-1 fibroblasts with iron oxide

Figure 3. MRI detection of systemic recruitment of fibroblasts into s.c. tumors. Tumors were initiated in the hind limb of CD-1 nude mice by s.c. inoculation of MLS cells (3×10^6) followed by a second i.p. injection of biotin-BSA-GdDTPA–labeled or unlabeled CV-1 fibroblasts (2×10^6; Table 1, *Exp IV, a*). *A,* R_1 maps of the tumor region overlaid on the corresponding grayscale images (flip angle of 15 degrees). *Left,* unlabeled CV-1 fibroblasts. *Right,* biotin-BSA-GdDTPA–labeled CV-1 fibroblasts. *B,* average R_1 values were obtained from regions of interest analysis of the tumor regions 2 to 7 d after injection of labeled (*black columns*) or unlabeled (*white columns*) mice fibroblasts [n = 5 for each group; *bars,* SE. *, $P < 0.05$, significant change in R_1 of labeled versus unlabeled tumors (unpaired one-tailed t test)]. *C,* T2* weighted MRI of tumor regions obtained 2 d after i.p. injection of Feridex labeled (*right*) or unlabeled (*left*) fibroblasts (Table 1, *Exp IV, b*). *Arrows,* Feridex-labeled fibroblasts at the tumor region. *D, top,* Prussian blue staining of tumor specimens after i.p. injection of Feridex-labeled fibroblasts. *Bottom,* costaining of Prussian blue and α-SMA.

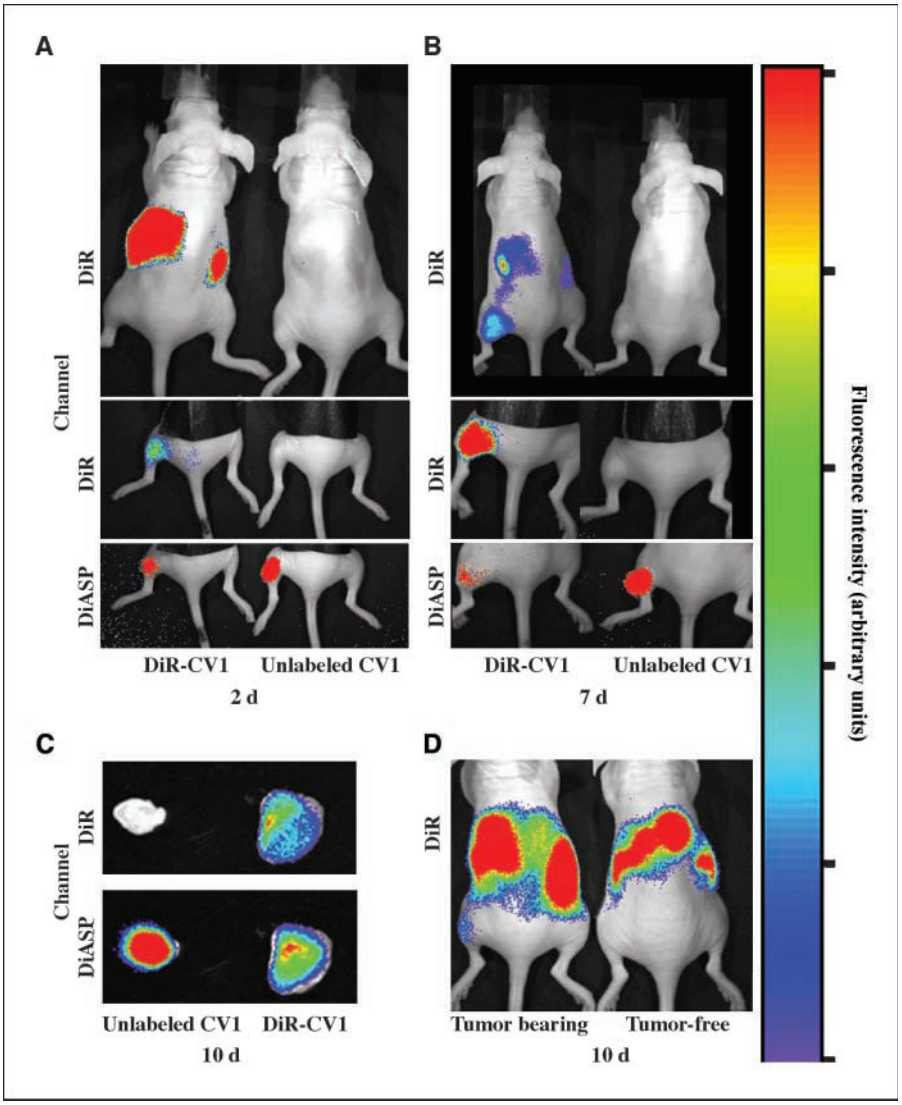

Figure 4. Recruitment of fibroblasts into s.c. tumors detected by near-IR fluorescence imaging. Tumors were initiated in the left hind limb of CD-1 nude mice by s.c. inoculation of MLS cells labeled with DiASP followed by a second i.p. injection of CV-1 fibroblasts (2×10^6) labeled with DiR or unlabeled cells (*left* and *right mice*, respectively; Table 1, *Exp V*). Color-coded near-IR fluorescent images were acquired by IVIS 100 (Xenogen) system and were overlaid on photographic images of s.c. tumors. *A* and *B,* mice were viewed using near-IR fluorescence (*top,* no masking; *middle,* black tape covering on the abdomen) as well as DiASP fluorescence imaging (*A* and *B, bottom*). Images were acquired 2 d (*A*) and 7 d (*B*) after fibroblast injection. *C,* excised tumors. *Top,* near-IR fluorescence imaging of MLS tumors derived from mice injected with DiR-labeled (*right*) and unlabeled (*left*) CV-1 cells. *Bottom,* DiASP fluorescence of the labeled MLS tumor cells. *D,* CV-1 fibroblasts labeled with DiR were injected into the peritoneum of a tumor-bearing mouse (*left mouse*, tumor located at the left limb) or to a control tumor-free mouse (*right mouse*). Mice were viewed 10 d after inoculation (*C* and *D*).

particles before their i.p. administration into tumor-bearing mice (Feridex; Table 1, *Exp IV*). Recruitment of iron oxide–loaded cells to the s.c. ovarian carcinoma tumors was detected *in vivo* by MRI (Fig. 3). Prussian blue staining of tumor specimens revealed the presence of iron oxide–loaded cells at the borders of the tumor (Fig. 3). These labeled stromal cells were elongated and possessed typical fibroblastic morphology (i.e., spindle shape with branched cytoplasm and elliptic nucleus). No iron oxide–labeled macrophages could be detected in the tumor or its vicinity. Costaining of histologic sections for α-SMA and Prussian blue suggested that at the edges of the tumor, the recruited fibroblasts were undifferentiated (α-SMA negative), whereas toward the tumor mass, they expressed α-SMA, a marker for their differentiation to myofibroblasts (Fig. 3*D, bottom*).

***In vivo* near-IR detection of systemic fibroblast recruitment into tumors.** The MRI results of systemic fibroblast recruitment into s.c. tumors were validated by near-IR fluorescence imaging (Table 1, *Exp V*). DiR-labeled fibroblasts (CV-1) were injected into the peritonea of nude mice bearing s.c. DiASP-labeled MLS tumors. Two days after fibroblast injection, near-IR fluorescence was not only detected at the peritoneum but was also evident at the tumor region (Fig. 4*A*). Initially, the high local signal at the peritoneum site of injection saturated the camera and prevented detection of the lower signal that evolved at the tumor site. Thus, covering the mouse abdomen with a black tape was essential to reveal the tumor fluorescence. However, 7 days after fibroblast injection, the fluorescence at the tumor location increased whereas the fluorescence at the peritoneum declined, and tumor-recruited fibroblasts could be visualized even without masking of the abdomen for visualization (Fig. 4*B*). Fluorescence imaging of both the DiASP-labeled tumor cells and the DiR-labeled fibroblasts confirmed spatial registration of the recruited fibroblasts to the tumor (Fig. 4*A* and *B, bottom*).

The near-IR fluorescence persisted throughout the 10 days of follow-up, a time at which mice were sacrificed and tissues were excised for *ex vivo* near-IR fluorescence imaging (Fig. 4*C*). Whereas DiASP fluorescence was detected in all tumors, DiR fluorescence was only detectable in tumors generated in mice that have received fibroblasts labeled with DiR. No fluorescence was detected from the contralateral limb. The role of the tumor in inducing fibroblast recruitment was shown by injection of DiR-labeled CV-1 fibroblasts into the peritoneum of a tumor-free mouse. In the absence of a

tumor, the near-IR labeled cells remained confined to the peritoneum site throughout the experimental period (10 days; Fig. 4*D*).

Distribution of fibroblasts in s.c. tumors after systemic recruitment. The finding that i.p. administered fibroblasts were recruited by the s.c. ovarian tumor intrigued us to further elucidate the spatial organization of these cells within the tumor. Thus, we analyzed the distribution of tumor cells, fibroblasts, and blood vessels by two-photon microscopy (Table 1, *Exp VI*; Fig. 5; Supplementary Figs. S2 and S3). Fluorescent MLS tumors were generated by s.c. inoculation of MLS ovarian cancer cells prelabeled with DiD (5×10^6 cells), followed 5 days later by i.p. injection of CV-1 fibroblasts prelabeled with CM-DiI or CFSE (2×10^6 cells; Fig. 5). Three days after i.p. administration of fibroblasts, mice were anesthetized and the vasculature was highlighted by i.v. injection of dextran-FITC into the tail vein (2 mg/mouse in 0.2 mL PBS). Mice were sacrificed 2 min afterwards and tumors were excised and visualized by two-photon microscopy. To image both the surface as well as the inner parts of the tumor, tumors that were carefully excised were sectioned in the center and both sides were imaged by two-photon microscopy. Recruited fibroblasts were predominantly present at the tumor rim (Fig. 5; Supplementary Fig. S3). Within this region, we could detect torturous capillaries, which are characteristic of tumor angiogenesis. Tumor cells, however, were not detected within this region (Fig. 5*A, inner part*; Supplementary data). Large dilated vessels were observed at

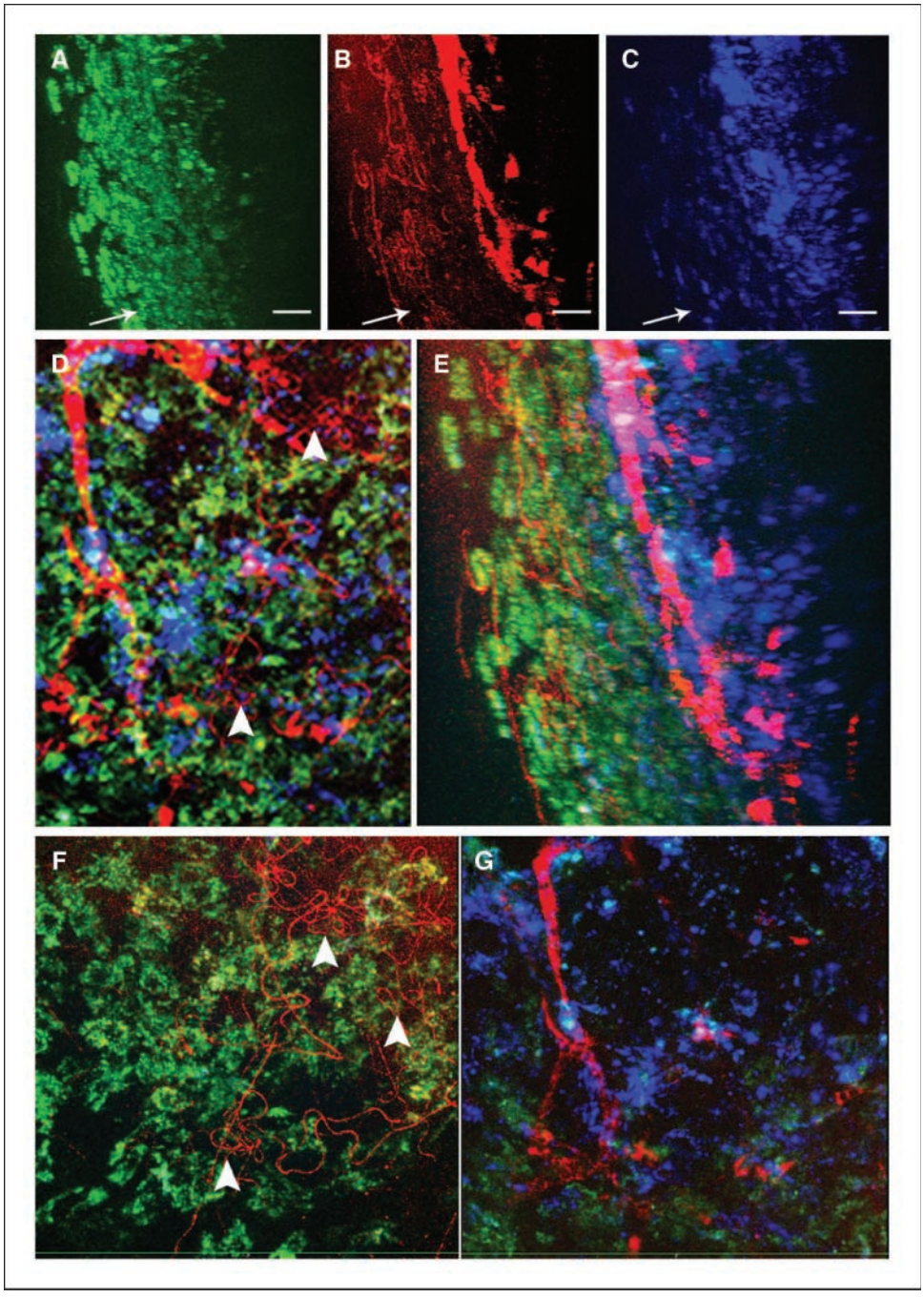

Figure 5. Two-photon microscopy of fibroblast distribution in s.c. MLS tumors. Two-photon microscopy of excised s.c. fluorescently labeled MLS tumors (Table 1, *Exp VI*). MLS tumor cells were labeled with DiD (*blue*); fibroblasts were labeled with CM-DiI (*green*); and blood vessels were visualized by i.v. injection of dextran-FITC (*red*). ZY projections of the entire 126 slices scanned presenting the fibroblast (*A*), vasculature (*B*), tumor cells (*C*), and the overlay (*E*). *Arrows,* tumor center. Bar, 35 μm. *D,* XY projection of the same 126 slices. *Arrowheads,* tortuous capillaries. *F,* XY projection of 42 of 126 outer slices (84 μm). *G,* XY projection of 56 of 126 inner slices (112 μm).

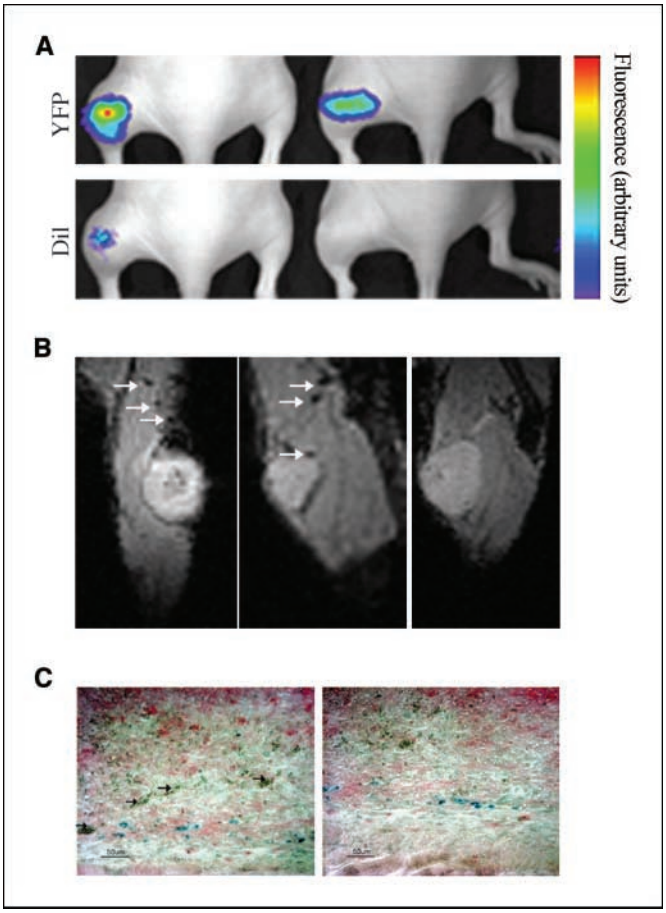

Figure 6. Recruitment of human primary fibroblasts into s.c. tumors (Table 1, *Exp VII*). *A,* tumors were initiated in the left hind limb of CD-1 nude mice by s.c. inoculation of MLS cells transfected with yellow fluorescent protein (*YFP*), followed by a second i.p. injection of WI38 fibroblasts (2×10^6) labeled with DiI (*left*) or unlabeled cells (*right*). *B,* tumors initiated by s.c. inoculation of MLS cells, followed by i.p. injection of PFN2 fibroblasts (1×10^6) labeled with Feridex (*left* and *middle*) or unlabeled cells (*right*). *Arrows,* hypointense regions correlating with Feridex-labeled PFN2 fibroblasts. *C,* Prussian blue and α-SMA costaining of tumor specimens that were excised from mice presented in (*B*). *Arrows,* blood vessels.

the tumor-fibroblast interface. The same pattern was observed with fibroblasts that were labeled with CFSE as well as for tumors coinoculated with fibroblasts. Whereas recruited fibroblasts were detected at the surface of the tumor, they were absent from the inner part of the tumor (supplementary Fig. S2). The desmoplastic reaction that developed in tumors of the recruitment studies resembled that observed in specimens obtained from s.c. tumors initiated exclusively from MLS cells (Fig. 1).

Primary human fibroblasts are systemically recruited into s.c. tumors. Recruitment and distribution of human primary fibroblasts were evaluated using breast- and lung-derived fibroblasts (PFN24 and WI38, respectively) that were i.p. given into mice bearing s.c. human epithelial ovarian carcinoma MLS tumors. PFN2 fibroblasts were labeled with SPIO particles for MRI and histochemical detection, whereas WI38 were labeled with DiI for fluorescence detection (Fig. 6). Recruitment of the human primary fibroblasts to the tumor could be detected by all three modalities. Prussian blue staining of these tumor specimens detected labeled human primary fibroblasts in close proximity to blood vessels at the tumor rim (Fig. 6*C, arrows*).

Discussion

During the last years, much evidence has been provided about the central contribution of the tumor microenvironment as a modulator of carcinogenesis through its influence on angiogenesis, progression, and malignancy of epithelial tumors. Reactive fibroblasts (i.e., myofibroblasts) are the major cellular constituent of the tumor-associated stroma and affect cancer progression (10, 47). We have previously shown that infiltration of myofibroblasts can contribute to stabilization of the neovasculature by expression of angiopoietin-1 and angiopoietin-2, and that their infiltration to the tumor provides the switch for exit from dormancy of implanted ovarian carcinoma spheroids (8, 9). To allow tracking of the recruitment of fibroblasts to tumors by MRI, we used the endogenous caveola-mediated uptake of albumin by fibroblasts to load cells with biotin-BSA-GdDTPA (43).

In the study reported here, we applied MRI and optical imaging for studying the recruitment of fibroblasts to human ovarian carcinoma tumors. MRI tracking of cell recruitment was achieved by labeling the fibroblasts with biotin-BSA-GdDTPA. The prolonged *in vivo* visibility of the signal arising from biotin-BSA-GdDTPA–loaded fibroblasts is consistent with our previous *in vitro* studies (43) and enabled serial *in vivo* follow-up of fibroblast migration and recruitment to the tumor. Local and systemic recruitment of fibroblasts to s.c. ovarian carcinoma xenografts was detected by MRI and validated by *in vivo* near-IR imaging, revealing labeled fibroblasts at the tumor region, whereas no labeled cells could be detected in the contralateral tumor-free limb or in limbs of tumor-free mice. The identity of the recruited cells was verified by administration of fibroblasts prelabeled with iron oxide particles that could be detected both by MRI and by Prussian blue staining of histologic sections. Labeled cells recruited to the tumor rim retained the typical spindle shape characteristic of fibroblasts, thus ruling out the option of secondary transfer of label to phagocytic macrophages.

Fibroblasts were previously shown to promote the invasion of endothelial cells into three-dimensional gel matrices (48), and infiltration of tumor fibroblasts was reported to facilitate and lead the angiogenic process (12, 14). The recruitment of iron oxide–labeled EPCs into s.c. glioma tumors was recently documented by susceptibility-weighted MRI (41). SPIO-prelabeled EPCs were detectable in tumors 3 days after administration of 3×10^6 labeled EPCs. The ability to detect EPCs labeled with SPIO by T_2* contrast and fibroblasts labeled with biotin-BSA-GdDTPA by T_1 contrast raises the possibility to simultaneously track the role of both cells in tumor angiogenesis and tumor progression by multiparametric MRI.

The ovarian carcinoma tumors studied in this work exhibited a characteristic desmoplasia phenotype regardless of whether tumor cells were inoculated alone or fibroblasts were injected either by coinoculation or by subsequent proximal (s.c.) or distant (i.p.) administration. These results suggest that the external administration of labeled fibroblast supplemented the recruitment of endogenous fibroblasts but did not significantly alter tumor biology.

The distribution of recruited fibroblasts within the tumor mass was studied by two-photon microscopy imaging and showed recruited fibroblasts primarily at the tumor rim, coinciding with tortuous neovasculature. As opposed to these small capillaries, dilated vessels were located at the tumor-fibroblast interface. This spatial difference in vascular morphology is consistent with our previous finding that VEGF in these tumors is predominantly

expressed by the MLS tumor cells whereas angiopoietin-1 and angiopoietin-2 are expressed by the stroma fibroblasts (9). The spatial organization of the recruited fibroblasts at the borders of the tumor and their colocalization with the neovasculature provide additional evidence for the role of these cells in stabilization of tumor-induced neovasculature. Additional chemoattractants, which could participate in this process, include fibroblast growth factor, PDGF, and tumor necrosis factor. Moreover, fibroblasts and myofibroblasts are known to express CXC chemokine ligand 12/stromal cell–derived factor-1 (49) that binds to its receptor CXCR4 on endothelial cells, which could then promote recruitment of endothelial cells to the rim of the tumor (12). Recruited fibroblasts may be stimulated by tumor-derived TGFβ1 to differentiate into myofibroblasts and then into pericyte-like cells, which would interact with the tumor neovasculature to stabilize the vessels and regulate blood flow. Indeed, costaining of tumor specimens for α-SMA expression and Prussian blue showed recruited, undifferentiated fibroblasts in close proximity to large blood vessels located at the tumor-host interface. However, in the vicinity of the tumor rim, these Prussian blue–positive fibroblasts additionally expressed α-SMA, thus indicating their differentiation into myofibroblasts. We thus suggest that i.p. administered fibroblasts reach the tumor area via the blood vessels, migrate into the tumor rim, and differentiate into myofibroblasts. The precise role of these cells within the tumor remains to be studied; however, multiple studies implicated infiltrating tumor myofibroblasts in the recruitment of endothelial cells and promotion of angiogenic sprouts as well as stabilization of tumor neovascularization. The ability to track these stroma cells would help in addressing the molecular mechanisms underlying their recruitment and role in tumor progression.

In summary, we report here the extensive recruitment of prelabeled fibroblasts into the rim of ovarian carcinoma tumors, which could be followed noninvasively by both MRI and optical imaging. Uncovering the functions of fibroblasts in cancer formation and understanding the mechanism of their association with tumor and endothelial cells, as well as with other components of the tumor microenvironment, are important due to the role of these cells in tumor progression. Furthermore, the ability to noninvasively follow these cells may potentially be beneficial for using the endogenous recruitment of fibroblasts to tumors for targeted image-guided cellular therapy.

Acknowledgments

Received 2/19/2007; revised 7/12/2007; accepted 7/20/2007.

Grant support: Israel Science Foundation grant 391/02 and National Cancer Institute grant R01 CA75334 (M. Neeman). M. Neeman is incumbent of the Helen and Morris Mauerberger Chair.

The costs of publication of this article were defrayed in part by the payment of page charges. This article must therefore be hereby marked *advertisement* in accordance with 18 U.S.C. Section 1734 solely to indicate this fact.

References

1. Ozols RF, Bookman MA, Connolly DC, et al. Focus on epithelial ovarian cancer. Cancer Cell 2004;5:19–24.
2. Ho SM. Estrogen, progesterone and epithelial ovarian cancer. Reprod Biol Endocrinol 2003;1:73.
3. Murdoch WJ, McDonnel AC. Roles of the ovarian surface epithelium in ovulation and carcinogenesis. Reproduction 2002;123:743–50.
4. Konishi I. Gonadotropins and ovarian carcinogenesis: a new era of basic research and its clinical implications. Int J Gynecol Cancer 2006;16:16–22.
5. Schiffenbauer YS, Abramovitch R, Meir G, et al. Loss of ovarian function promotes angiogenesis in human ovarian carcinoma. Proc Natl Acad Sci U S A 1997;94:13203–8.
6. Schiffenbauer YS, Meir G, Maoz M, Even-Ram SC, Bar-Shavit R, Neeman M. Gonadotropin stimulation of MLS human epithelial ovarian carcinoma cells augments cell adhesion mediated by CD44 and by α(v)-integrin. Gynecol Oncol 2002;84:296–302.
7. Gilead A, Neeman M. Dynamic remodeling of the vascular bed precedes tumor growth: MLS ovarian carcinoma spheroids implanted in nude mice. Neoplasia 1999;1:226–30.
8. Gilead A, Meir G, Neeman M. The role of angiogenesis, vascular maturation, regression and stroma infiltration in dormancy and growth of implanted MLS ovarian carcinoma spheroids. Int J Cancer 2004;108:524–31.
9. Gilad AA, Israely T, Dafni H, Meir G, Cohen B, Neeman M. Functional and molecular mapping of uncoupling between vascular permeability and loss of vascular maturation in ovarian carcinoma xenografts: the role of stroma cells in tumor angiogenesis. Int J Cancer 2005;117:202–11.
10. Bissell MJ, Labarge MA. Context, tissue plasticity, and cancer: are tumor stem cells also regulated by the microenvironment? Cancer Cell 2005;7:17–23.
11. De Wever O, Mareel M. Role of tissue stroma in cancer cell invasion. J Pathol 2003;200:429–47.
12. Orimo A, Gupta PB, Sgroi DC, et al. Stromal fibroblasts present in invasive human breast carcinomas promote tumor growth and angiogenesis through elevated SDF-1/CXCL12 secretion. Cell 2005;121:335–48.
13. Tuxhorn JA, McAlhany SJ, Dang TD, Ayala GE, Rowley DR. Stromal cells promote angiogenesis and growth of human prostate tumors in a differential reactive stroma (DRS) xenograft model. Cancer Res 2002;62:3298–307.
14. Walter-Yohrling J, Pratt BM, Ledbetter S, Teicher BA. Myofibroblasts enable invasion of endothelial cells into three-dimensional tumor cell clusters: a novel *in vitro* tumor model. Cancer Chemother Pharmacol 2003;52:263–9.
15. Bagley RG, Weber W, Rouleau C, Teicher BA. Pericytes and endothelial precursor cells: cellular interactions and contributions to malignancy. Cancer Res 2005;65:9741–50.
16. Bhowmick NA, Neilson EG, Moses HL. Stromal fibroblasts in cancer initiation and progression. Nature 2004;432:332–7.
17. Kunz-Schughart LA, Knuechel R. Tumor-associated fibroblasts (part II): Functional impact on tumor tissue. Histol Histopathol 2002;17:623–37.
18. Mueller MM, Fusenig NE. Friends or foes—bipolar effects of the tumour stroma in cancer. Nat Rev Cancer 2004;4:839–49.
19. Kalluri R, Zeisberg M. Fibroblasts in cancer. Nat Rev Cancer 2006;6:392–401.
20. Orimo A, Tomioka Y, Shimizu Y, et al. Cancer-associated myofibroblasts possess various factors to promote endometrial tumor progression. Clin Cancer Res 2001;7:3097–105.
21. Bergers G, Benjamin LE. Tumorigenesis and the angiogenic switch. Nat Rev Cancer 2003;3:401–10.
22. Martin TA, Harding KG, Jiang WG. Regulation of angiogenesis and endothelial cell motility by matrix-bound fibroblasts. Angiogenesis 1999;3:69–76.
23. Wenger A, Kowalewski N, Stahl A, et al. Development and characterization of a spheroidal coculture model of endothelial cells and fibroblasts for improving angiogenesis in tissue engineering. Cells Tissues Organs 2005;181:80–8.
24. Kunz-Schughart LA, Heyder P, Schroeder J, Knuechel R. A heterologous 3-D coculture model of breast tumor cells and fibroblasts to study tumor-associated fibroblast differentiation. Exp Cell Res 2001;266:74–86.
25. Kunz-Schughart LA, Schroeder JA, Wondrak M, et al. Potential of fibroblasts to regulate the formation of three-dimensional vessel-like structures from endothelial cells *in vitro*. Am J Physiol Cell Physiol 2006;290:C1385–98.
26. Elenbaas B, Weinberg RA. Heterotypic signaling between epithelial tumor cells and fibroblasts in carcinoma formation. Exp Cell Res 2001;264:169–84.
27. Tomasek JJ, Gabbiani G, Hinz B, Chaponnier C, Brown RA. Myofibroblasts and mechano-regulation of connective tissue remodelling. Nat Rev Mol Cell Biol 2002;3:349–63.
28. Direkze NC, Hodivala-Dilke K, Jeffery R, et al. Bone marrow contribution to tumor-associated myofibroblasts and fibroblasts. Cancer Res 2004;64:8492–5.
29. Roni V, Habeler W, Parenti A, et al. Recruitment of human umbilical vein endothelial cells and human primary fibroblasts into experimental tumors growing in SCID mice. Exp Cell Res 2003;287:28–38.
30. Indraccolo S, Moserle L, Tisato V, et al. Gene therapy of ovarian cancer with IFN-α-producing fibroblasts: comparison of constitutive and inducible vectors. Gene Ther 2006;13:953–65.
31. Desmouliere A, Guyot C, Gabbiani G. The stroma reaction myofibroblast: a key player in the control of tumor cell behavior. Int J Dev Biol 2004;48:509–17.
32. Ishii G, Sangai T, Oda T, et al. Bone-marrow-derived myofibroblasts contribute to the cancer-induced stromal reaction. Biochem Biophys Res Commun 2003;309:232–40.
33. Sangai T, Ishii G, Kodama K, et al. Effect of differences in cancer cells and tumor growth sites on recruiting bone marrow-derived endothelial cells and myofibroblasts in cancer-induced stroma. Int J Cancer 2005;115:885–92.
34. Ishii G, Sangai T, Ito T, et al. *In vivo* and *in vitro* characterization of human fibroblasts recruited selectively into human cancer stroma. Int J Cancer 2005;117:212–20.
35. Serini G, Gabbiani G. Mechanisms of myofibroblast activity and phenotypic modulation. Exp Cell Res 1999;250:273–83.
36. Kircher MF, Allport JR, Graves EE, et al. *In vivo* high resolution three-dimensional imaging of antigen-specific cytotoxic T-lymphocyte trafficking to tumors. Cancer Res 2003;63:6838–46.

37. Huber MM, Staubli AB, Kustedjo K, et al. Fluorescently detectable magnetic resonance imaging agents. Bioconjug Chem 1998;9:242–9.
38. Bhorade R, Weissleder R, Nakakoshi T, Moore A, Tung CH. Macrocyclic chelators with paramagnetic cations are internalized into mammalian cells via a HIV-tat derived membrane translocation peptide. Bioconjug Chem 2000;11:301–5.
39. Crich SG, Biancone L, Cantaluppi V, et al. Improved route for the visualization of stem cells labeled with a Gd-/Eu-chelate as dual (MRI and fluorescence) agent. Magn Reson Med 2004;51:938–44.
40. Anderson SA, Glod J, Arbab AS, et al. Noninvasive MR imaging of magnetically labeled stem cells to directly identify neovasculature in a glioma model. Blood 2005; 105:420–5.
41. Arbab AS, Frenkel V, Pandit SD, et al. Magnetic resonance imaging and confocal microscopy studies of magnetically labeled endothelial progenitor cells trafficking to sites of tumor angiogenesis. Stem Cells 2006; 24:671–8.
42. Geninatti Crich S, Bussolati B, Tei L, et al. Magnetic resonance visualization of tumor angiogenesis by targeting neural cell adhesion molecules with the highly sensitive gadolinium-loaded apoferritin probe. Cancer Res 2006;66:9196–201.
43. Granot D, Kunz-Schughart LA, Neeman M. Labeling fibroblasts with biotin-BSA-GdDTPA-FAM for tracking of tumor-associated stroma by fluorescence and MR imaging. Magn Reson Med 2005;54:789–97.
44. Silzle T, Kreutz M, Dobler MA, Brockhoff G, Knuechel R, Kunz-Schughart LA. Tumor-associated fibroblasts recruit blood monocytes into tumor tissue. Eur J Immunol 2003;33:1311–20.
45. Dafni H, Landsman L, Schechter B, Kohen F, Neeman M. MRI and fluorescence microscopy of the acute vascular response to VEGF165: vasodilation, hyperpermeability and lymphatic uptake, followed by rapid inactivation of the growth factor. NMR Biomed 2002;15: 120–31.
46. Kalchenko V, Shivtiel S, Malina V, et al. Use of lipophilic near-infrared dye in whole-body optical imaging of hematopoietic cell homing. J Biomed Opt 2006;11:050507.
47. Bissell MJ, Radisky D. Putting tumours in context. Nat Rev Cancer 2001;1:46–54.
48. Dietrich F, Lelkes PI. Fine-tuning of a three-dimensional microcarrier-based angiogenesis assay for the analysis of endothelial-mesenchymal cell cocultures in fibrin and collagen gels. Angiogenesis 2006; 9:111–25.
49. Orimo A, Weinberg RA. Stromal Fibroblasts in Cancer: A Novel Tumor-Promoting Cell Type. Cell Cycle 2006;5:1597–601.